Superelasticity and Nanofracture Mechanics of ZnO Nanohelices

Pu Xian Gao, Wenjie Mai, and Zhong Lin Wang*

School of Materials Science and Engineering, Georgia Institute of Technology, Atlanta, Georgia 30332-0245

ABSTRACT

A superelasticity (shape memory) behavior has been discovered for the superlattice-structured ZnO nanohelices. By in situ manipulation using a nanoprobe, the nanohelix could elastically recover its shape after an extremely large axial stretching to a degree close to the theoretical limit, while suffering little residual plastic deformation. As a result, its spring constant can be increased continuously for up to 300−800%. A shape memory/recovery of the nanohelix was observed after subjecting to a buckling deformation. The superelastic deformation and fracture process of a nanohelix have been studied by transversely compressing under an AFM tip. A two-step mechanism is suggested for explaining the measured force-displacement curve. It is suggested that the small thickness and the superlattice structure of the nanohelix might be the keys for the observed superelasticity. The ZnO nanohelices may be a new category of shape-memory ceramic nanostructures, which could be of great interest for investigating nanoscale fracture process and application in MEMS and NEMS. The elastic recovery of the nanohelix after extremely large deformation makes it a potential structure for nanoscale elastic energy storage.

As a unique three-dimensional object, helical/spring structures, either in micro- or nanoscale, have been found for a number of materials, such as C,[1,2] Si/Ge,[3−5] SiO$_2$,[6,7] SiC,[8] ZnO,[9−12] InP,[13] and InGaAs/GaAs,[14,15] which are unique structures with potential applications in electronics, optoelectronics, sensing and actuating, and electromechanically coupled nanodevices. Consequently, helical nanostructures of piezoelectric and semiconducting zinc oxide (ZnO), such as nanorings[10,11] and nanosprings,[9,11,12] have drawn extensive research interest. Our recent discovery of the superlattice-structured ZnO nanohelices[16] presents a brand-new helical nanostructure that is composed of two types of alternating and periodically distributed long crystal stripes, oriented with their *c* axes normal to each other.

In this paper, the superelasticity and nanoscale fracture behavior of the ZnO nanohelix have been studied by two independent techniques: in situ stretching and compressing in SEM, and atomic force microscopy (AFM) compression. A shape recovery from a buckling deformation of the nanohelix was observed. The fracture process of the nanohelix reveals a two-step process, which has been explained by the buckling process.

Superelasticity. The superlattice-structured ZnO nanohelices were grown using a vapor−solid process, and their growth structure has been analyzed in details, as reported previously.[16] Before the mechanical manipulation, the nanohelices were first transferred from the original polycrystalline alumina substrate onto other platforms such as a flat Si substrate and a lacey carbon transmission electron micros-

copy (TEM) grid. The mechanical property was studied using a nanomanipulator inside a focused ion beam microscope (FIB, FEI NOVA 200). In the FIB system, the nanohelix was picked up by welding its one end using platinum (Pt) deposition onto the tip of a tungsten nanoprobe (∼100 nm in diameter at the tip), which was mounted on the nanomanipulator. The manipulation experiments were carried out via extending or compressing the nanohelix using the nanoprobe tip.

Figure 1a−c is a series of SEM images of the grown nanohelices of ZnO. Figure 1a displays a relaxed, straight, and right-handed nanohelix lying on a Si substrate, which is ∼560 nm in diameter, ∼1.8 μm in pitch, and ∼440 nm in width. TEM characterization has confirmed its superlattice structure as reported previously.[16] In some cases, an as-grown nanohelix could be naturally bent and twisted for ∼180° without breaking (Figure 1b). When the nanohelices were transferred onto a flat Si (100) substrate, the adhesion force between the nanohelix and the Si substrate can make the nanohelix "self-bent" for ∼180° (Figure 1c). The curly nanobelt is made of a periodic, coherent, epitaxial, and parallel assembly of two alternating stripes of zinc oxide crystals oriented with their *c* axes perpendicular to each other. The rigid structural rotation/twist caused by the superlattice results in the initiation and formation of the nanohelix.[16]

For the in situ manipulation inside the FIB system, the extension or compression of a nanohelix by a tungsten nanoprobe was recorded continuously through SEM imaging. Figure 2 shows a series of snapshot SEM images displaying a mechanical loading process by the nanoprobe onto a nanohelix. In Figure 2a, two nanohelices have been trans-
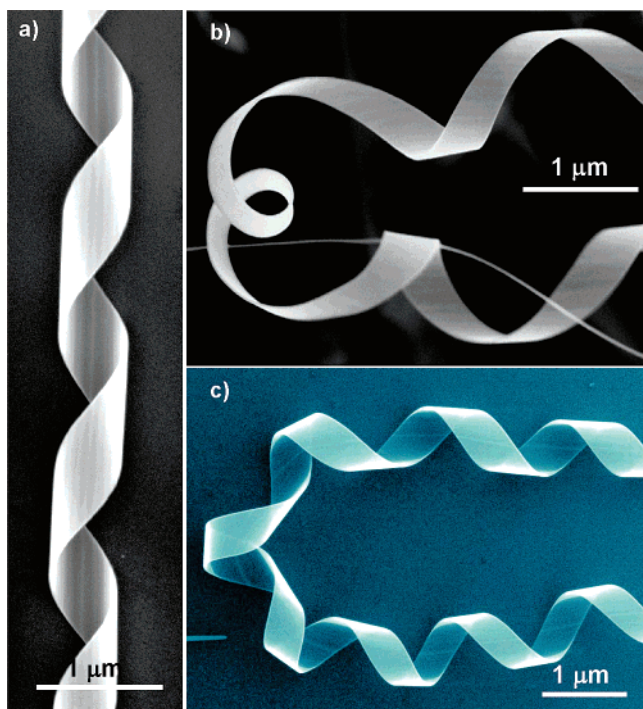
Figure 1. Series of SEM images of superlattice-structured ZnO nanohelices. Parts a and b are, respectively, a relaxed and straight nanohelix and a full arch nanohelix. (c) A manipulated arch of nanohelix by adhesion force from the contact with Si substrate.

Figure 2. Manipulation process of a nanohelix upon an extremely large axial stretching and shape-recovery process. The nanohelix was deposited on silicon substrate. (a) One end of a nanohelix was welded with Pt onto a tungsten nanoprobe. (b) An attempt for extracting the welded nanohelix out of the entangled nanohelices. (c) An enlarged SEM image showing the extremely stretched nanohelix. (d) Continued extraction led to an initial release of the welded nanohelix from the entangled point and a recovery of the nanohelix shape. (e) A complete restoring of the nanohelix shape after the manipulation in b and c, suggesting a superelasticity (shape memory) behavior.

ferred onto a Si substrate and entangled to each other with a cross-knot position, as indicated by an arrowhead. The white arrowhead points to one end of a nanohelix that was welded onto the tungsten nanoprobe using the ion-beam-induced Pt deposition. To avoid or reduce the damage from the ion beam, the lowest current available for Pt deposition was used. Despite the entanglement between the two nanohelices, the two nanohelices can be distinguished easily in Figure 2a. The dimensions of the welded nanohelix are approximately 1 μm in diameter, 2.2 μm in pitch, and 220 nm in width. To pull the welded nanohelix out of the cross-knot, the nanoprobe gradually extended the welded nanohelix away from the other one. In reference to the position marked by the arrowhead, it is amazing to find that the welded nanohelix can be pulled to an almost straightened shape, while its twist cycles are preserved. The enlarged image in Figure 2c reveals that the extended nanohelix has reached an extreme extension, for which the width of the nanobelt decreased to ~190 nm, less than the original width of 220 nm, indicating a curly bending of the nanobelt across its width under external mechanical stretching.

A continued stretching manipulation of the nanoprobe has led to the sliding of the cross-knot from its original position in Figure 2b to an unknotted position as marked in Figure 2d. The entangled position is marked with a dashed arrow. Obviously, the stretched nanohelix has begun to recover its shape from the extreme extension displayed in Figure 2b and c. Further manipulation has pulled the welded nanohelix completely away from the unwelded one, as shown in Figure 2e. A careful comparison to the nanohelix dimensions presented in Fig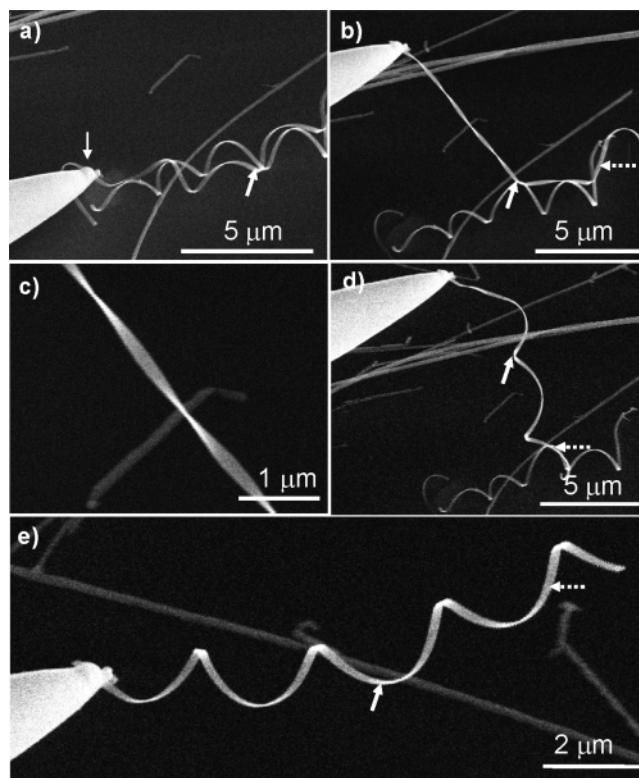ure 2a indicates that the nanohelix has an almost identical dimensionality including pitch and radius, suggesting a complete elastic recovery, that is, a superelasticity (shape memory) behavior.

To confirm such an effect, another nanohelix was mechanically manipulated on a lacey carbon grid. Because of the local contact adhesion between the nanohelix and the copper grid, a clamped end was formed as marked by an arrowhead in Figure 3a. It is obvious that the left-hand half of the nanohelix from the clamped point had been stretched by the manipulation probe, while the right-hand half remained unchanged and kept the original dimensions of 1.1 μm in diameter, 3.6 μm in pitch, and 500 nm in width. Gradual extension proceeded as shown in Figure 3b to an extreme extension in Figure 3c, which gave rise to a diameter decrease in the width of the nanohelix, 500 nm, nearly forming a straightened nanobelt. After breaking from the contact adhesion point between the nanohelix and copper grid by mechanical pulling, the nanohelix had the other end completely free (Figure 3d), following which there was a damped axial resonance of the nanohelix, and the SEM image only caught some moments of the vibration because of slower scan speed (Figure 3e). Finally, it recovered its original dimension with a uniform pitch and diameter throughout the entire nanohelix.
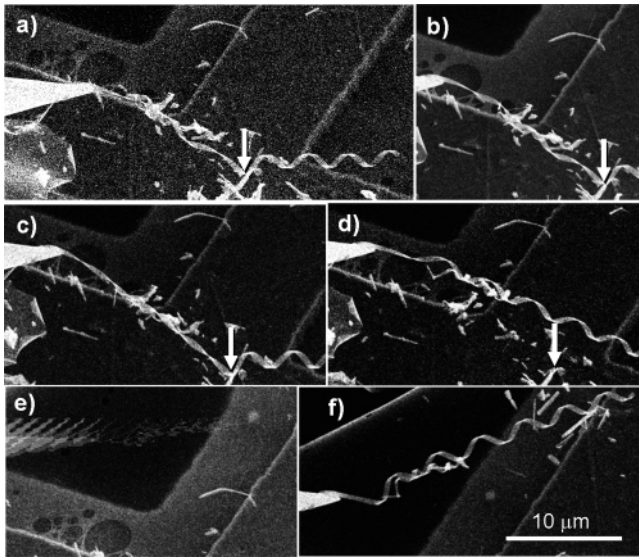
Figure 3. Another manipulation process of a nanohelix under an extremely large extension and superelastic recovery in its shape. The nanohelix was deposited on a TEM grid coated with carbon film. (a) A welded nanohelix on a tungsten nanoprobe was stretched partially with a clamped end in the middle part of the nanohelix due to the local sticking of the nanohelix with the grid. (b) An enlarged SEM image showing the transition position from the stretched part (left-hand side) of the nanohelix to the unstretched part (right-hand side). (c) An extreme large extension led to the straightening of the nanohelix and reducing in diameter. (d) An initial recovery of the nanohelix from the extreme extension after overcoming the adhesion from the grid surface. (e) A resonance recovery was captured with unresolved trace because of the slower scanning speed of the SEM. (f) A complete elastic recovery of the extremely extended nanohelix to its original shape with uniform pitches through the entire length.

To see if a compression load would lead to a similar mechanical behavior, a compression manipulation by a nanoprobe was conducted on another welded nanohelix. The nanohelix had dimensions of 300 nm in diameter, 1 μm in pitch distance, and 380 nm in width. Figure 4 records the sequential images of the nanohelix during compression loading and after releasing on the load. With the gradual increase of the loading by the nanoprobe, compression deformation produced a shortening and twisting of the nanohelix (Figure 4a−d). When the contact adhesion between the nanohelix and the carbon film could not bare the load from the nanoprobe, the nanohelix broke off from the substrate and remained free in air (Figure 4e). The deformed nanohelix eventually restored its original shape (Figure 4f), suggesting an elastic deformation during the compression.

Figure 5 records an elastic deformation and recovery process with a buckling deformation phenomenon for a nanohelix compressed by a tungsten nanoprobe. Starting from the edge of one end of a nanohelix lying on flat Si substrate (Figure 5a), the nanoprobe tip was manipulated close to the edge (Figure 5b). A compressing operation by manipulator enabled the probe tip to contact the nanohelix front edge (Figure 5c) and deform it significantly at the edge (Figure 5d). As indicated by an arrowhead, the nanoscale local buckling and recovery of the nanohelix are shown from Figure 5e−j. The hanged side of the coiled nanobelt was

compressed to become flatter and flatter (Figures 5e−g), until being bent over and buckled (Figure 5h), where an inward arched deformation was formed from the side of the coiled nanobelt. The release of the load on the edge led to the recovery of the deformed nanohelix, especially the buckled position as indicated by an arrowhead. Comparing to the original shape in Figure 5a, the buckled position of the recovered nanohelix has an almost identical shape. Also, it is unlikely to have dislocations created by the deformation due to the small thickness (20 nm) of the nanohelix; the data suggest a possible nanoscale elastic buckling and recovery process of the nanohelix when subject to a transverse tip compression.

To describe the mechanism involved in the reversible, extremely large extension and compression of the nanohelix, that is, the superelasticity (shape memory) effect, a mechanical model of the nanohelix was established as shown in Figure 6a and b. For a nanohelix with original dimensions of $2r_o$ in diameter, H_o in pitch distance, a in thickness, and b in width (Figure 6a), upon uniaxial load F, either for compression or extension, the mechanical response can be divided into four terms, as shown schematically in Figure 6b: shear force Q_f and tension force N_f as the orthogonal divisions from the uniaxial force F, and the bending moment M_{Nf} as well as torsion moment T_{Qf}. In this case, the ends of the nanohelix are free to rotate, and there is no need to consider the friction-induced fixation momentum at the ends.

Assuming that a uniaxial force was applied on a nanohelix and considering geometric symmetry of the nanohelix, we take one cycle of the nanohelix as a unit for the calculation. On the basis of Hookes' law and the principle of virtual work,[17,18] and using classical elasticity theory, the spring constant, K, of the ZnO nanohelix can be derived as a function of its dimensions, tensile modulus E, and shear modulus G[19]

$$\frac{1}{K} = \frac{h^2}{l_0 EA} + \frac{4\pi^2 \alpha_s r^2}{l_0 GA} + \frac{h^2 r^2}{l_0 EI} + \frac{4\pi^2 r^4}{l_0 GJ} \qquad (1)$$

where h and r are, respectively, the instant pitch and instant radius of the nanohelix in the course of axial deformation, and $h = \sqrt{l_0^2 - 4\pi^2 r^2}$. α_s is the shear coefficient, which equals to $(7 + 6v)/(6(1 + v))$, v is the Poisson's ratio ($\sim$0.30 for ZnO), and l_o is the total length of a unit cycle of the coiled nanobelt, $l_0 = \sqrt{4\pi^2 r_0^2 + H_0^2}$, which is assumed to be a constant during the extension and compression of the nanohelix. The tensile modulus $E = 2(1 + v)G$. A is the cross-sectional area of the coiled nanobelt, I is the moment of inertia, and J is the polar moment of inertia of the cross section. For the superlattice-structured nanohelices, the coiled nanobelt has a rectangular cross section, so

$$A = ab, \quad I = \frac{1}{12}ba^3, \quad J = \frac{1}{12}ab(a^2 + b^2) \qquad (2)$$

r_0, a, and b can be extracted from the SEM image during nanohelix manipulation. Combining eqs 1 and 2, the spring
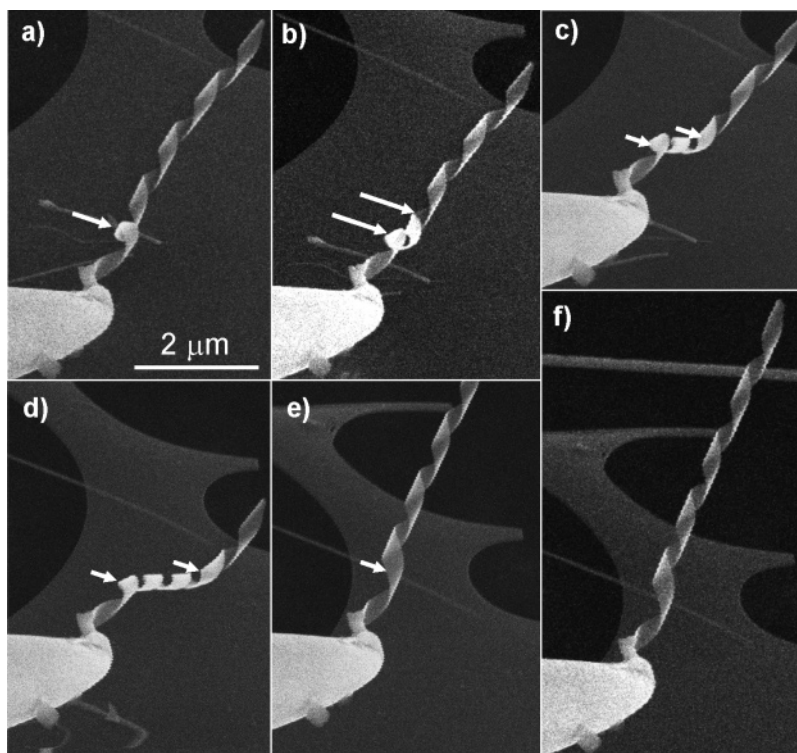
Figure 4. Compressed deformation process of a nanohelix induced by the nanoprobe. The compression-led shortening and twisting are indicated by arrowheads, starting from (a) a half-turn of the nanohelix; (b) one and half turns; (c) two turns; and (d) two and a half turns. (e) The nanohelix elastically jumped away from the contact point with the other end free because of an overload by the probe. (f) The nanohelix eventually restored its original shape, suggesting an elastic deformation during the compression.

constant of the nanohelix can be expressed as a function of the radius and shear modulus:

$$\frac{G}{K} = \frac{4\pi^2}{abl_0}\left[\frac{l_0^2 - 4\pi^2 r^2}{8\pi^2(1+v)a^2}(a^2+12r^2) + r^2\left(\frac{7+6v}{6(1+v)} + \frac{12r^2}{a^2+b^2}\right)\right] \quad (3)$$

Another assumption is that the shear modulus of the ZnO nanohelix is constant during the deformation process, ∼70 GPa.[20,21] So the dynamic spring constant of a deformed nanohelix depends on its instantaneous radius, thickness, and width. Because of the rather small thickness of the nanohelix (∼20 nm) compared to the radius (150−500 nm),[16] the effect of the thickness and width variations are negligible upon extension or compression. Therefore, the instant spring constant of a single nanohelix is tunable with a dynamic radius change during extension and compression.

On the basis of the experimental data acquired from the nanohelix manipulation, five sets of nanohelix dimensions have been used for numerical analysis on the radius dependence of the spring constant upon extension or compression. Figure 6c shows plots of spring constant versus instant radius of the five deformed nanohelices. The first three sets of nanohelices ($N_1 = 2, 3, 4$) are, respectively, from those illustrated in Figures 2, 3, and 4, which were plotted using black, green, and blue lines, respectively; the other two ($N_1 = 1, 5$) are from the average dimensions, which were plotted using red and pink solid lines, respectively.

Upon extension, the radius of the nanohelix decreases as the pitch is increased, while a compression would lead to an increase of the nanohelix radius as the pitch decreases.

With the black curve in Figure 6c and the inset plot representing the case presented in Figure 2, it is clearly seen that the spring constant remains fairly constant when the radius changes from $r = 350$ nm in stretching to $r = 530$ nm in compressing for the nanohelix with an original strain free radius of $r_o = 490$ nm, suggesting a small strained regime; thus, the deformation is dominated by the linear elastic process. While upon an extremely large extension, the nanohelix spring constant increases nonlinearly with a dramatic increase from 0.08 to 0.75 N/m (∼810% increase). The experimental elongation in the case of Figure 2 is ∼70%, very close to the theoretical limiting elongation of 72% given that the helical nanobelt can be stretched into a flat and straight nanobelt.

Table 1 summarizes the nanohelix elongation and spring constant increase as a result of maximum extensions in Figures 2, 3, and possibly 4. It is seen that upon extreme extensions the nanohelix becomes stiff with the radius decrease. Upon a corresponding experimental elongation close to the theoretical limit, the tunable spring constant increases by 300−800% (Table 1). It is also noticed that the static spring constant of a relatively tightly packed nanohelix such as the case in Figure 4 ($N_1 = 4$) is relatively large, 2.7 N/m. Under a possible extreme extension condition, its spring constant would have a 650% increase up to 20.3 N/m.

It is worth pointing out that the calculation model for the extension and compression here is based on a nanohelix with
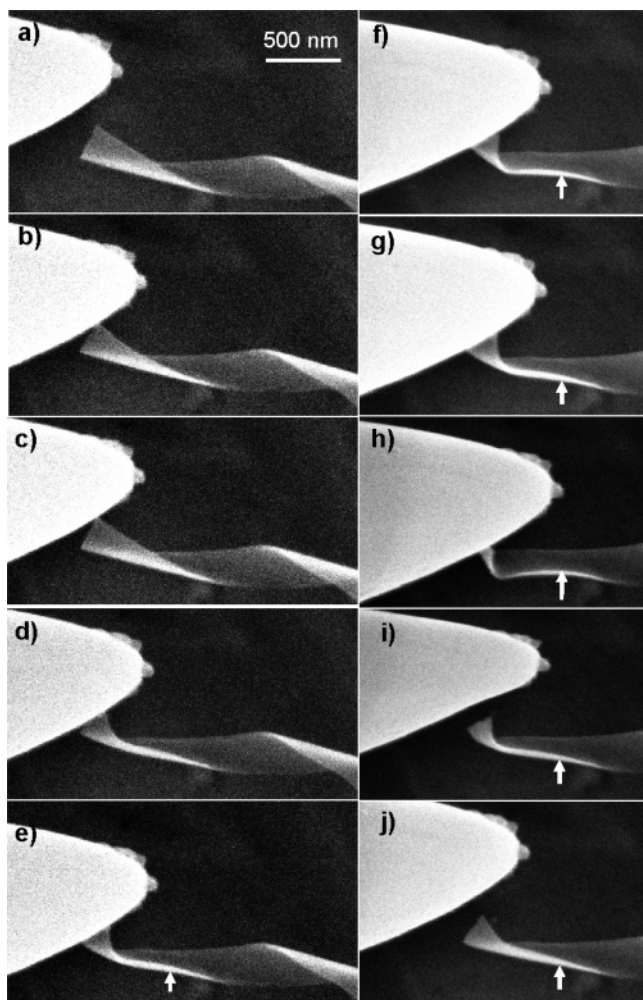
Figure 5. Elastic deformation and recovery process revealing a buckling phenomenon for a nanohelix pressed by a tungsten nanoprobe. The arrowhead indicates the local buckling and recovery part of the nanohelix from e to j.

ends free to rotate. For simplification purposes, only the moments and forces derived from the uniaxial force along the axial direction are considered. The calculated results revealed the dynamic change of the nanohelix diameter as well as its tunable dynamic spring constant. But when the fixation moment to the end is considered, the diameter change will be constrained as a function of the pitch angle change.[18] It will produce a certain deviation from the calculated results presented here. Considering the experimental observation of the extension and compression, it is reasonable to say that the manipulated nanohelices have the two ends free to rotate. There are two cases in which one might need to consider the fixation moment. One is when the stretching is close to the maximum elongation, there could be a fixation moment to be taken into account. The other is the compressing manipulation when the friction between the nanohelix end and the against membrane or object is large enough to hold the end from rotation.

Nanoscale Fracture. The second part of the experiments was carried out using an atomic force microscope (Molecular Force Probe MFP-3D from Asylum Research), which was used to transversely compress a nanohelix until fracture

occurred. Figure 7a and b are, respectively, an AFM topography image of a nanohelix after being compressed by the AFM tip and a corresponding SEM image. The measured force-displacement curves for a group of nanohelices are shown in Figure 7c. A common factor for the fracture of the nanohelices is that the force-displacement presents two sharp drops at F_1 and F_2, the values of which depend on the size of the nanohelix. A complete fracture of the nanohelix follows the sharp drop at F_2.

In Figure 5, we have found that a nanoscale elastic buckling deformation is possible upon compression. In the buckling process of a thin millimeter-scale elastic plate arch, the fracture mechanics has suggested a force drop to a smaller value due to a transition from stretching deformation to pure bending deformation.[22] For a transverse compression of the nanohelix, a two-step fracture process involving a nanoscale buckling phenomenon can be proposed for explaining the experimental data shown in Figure 7a−c.

Table 2 lists the characteristic forces for the 7 sets of transverse compression and fracture experiments conducted for the nanohelices of different dimensionality as plotted in Figure 7c. These nanohelices have a belt width ranging from 380−600 nm (much larger than the AFM tip radius of ∼50 nm), a diameter ranging from 900−1100 nm, and a pitch distance ranging from 1700−3800 nm. During the experiments, except for nanohelix no. 2 ($N_2 = 2$), all of the other nanohelices have been found to have the second drop in force, corresponding to occurrence of fracture. The final sudden increase in force is the result of tip touching the substrate.

The proposed fracture process is presented in Figure 7d. The nanohelix deformation process was represented by four instant cross-sectional views perpendicular to the axis of the nanohelix upon the AFM tip compression, a deformation process with four stages I, II, III, and IV. The four stages illustrate a two-step fracture process, that is, a prebuckling (stretching resistant) and then buckling (bending resistant) process. The prebuckling step is an elastic compression from stage I to stage II, representing compressing a circular nanohelix into an elliptical cross-section shape. Further compression will likely result in the initiation of the buckling, similar to the case presented in Figure 5e−g. The buckling stage is steps III and IV. As the deformation transitioned from stretching energy dominant to bending energy dominant, there was a sudden softening of the nanohelix, leading to a force drop at a steep rate at the vicinity of F_1. A continuous compressing leads to the eventual fracture of the nanohelix at the tip contact point at a force F_2. Because of the pyramid shape of the AFM tip with a tip radius of ∼50 nm, a local fracture resulted from the buckled plastic deformation by the tip is revealed in Figure 7b. Take nanohelix no. 1 ($N_2 = 1$) as an example (dark-lined force-displacement curve in Figure 7c) at $F_1 = 0.61$ μN with a displacement of 115 nm, the force drop occurred as a buckling deformation being initiated (from stage II to III) as a result of transition from stretching resistant deformation to bending dominant. The bending resistance will lead to a later sustained force curve until the tip displacement reached
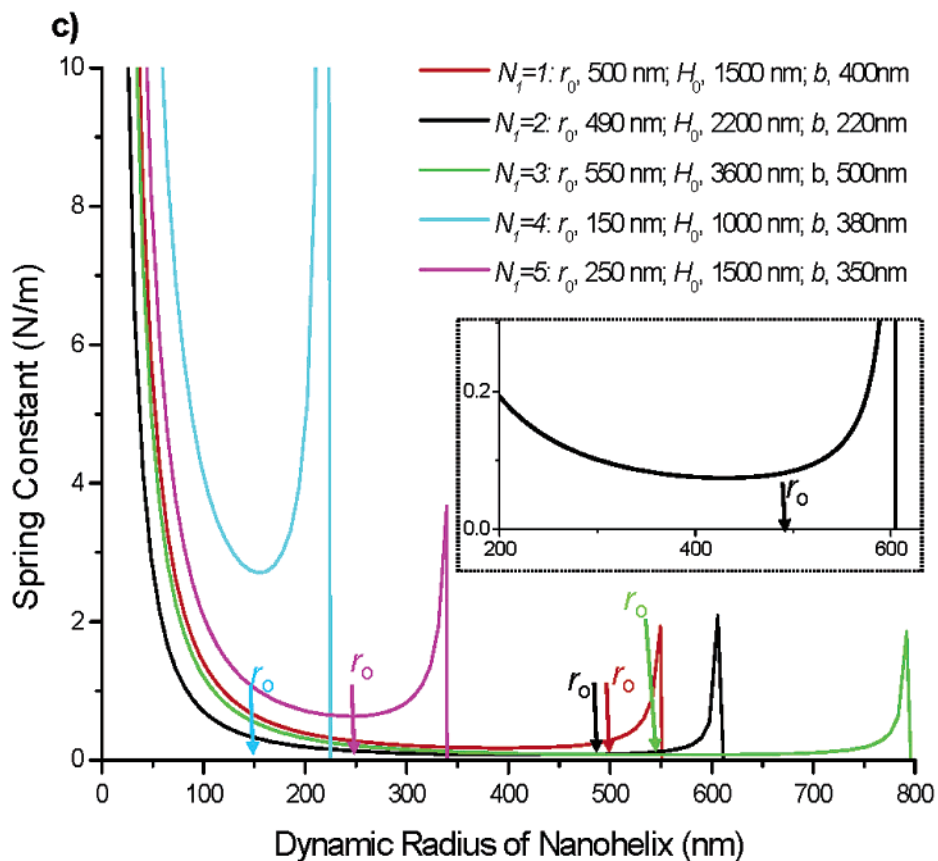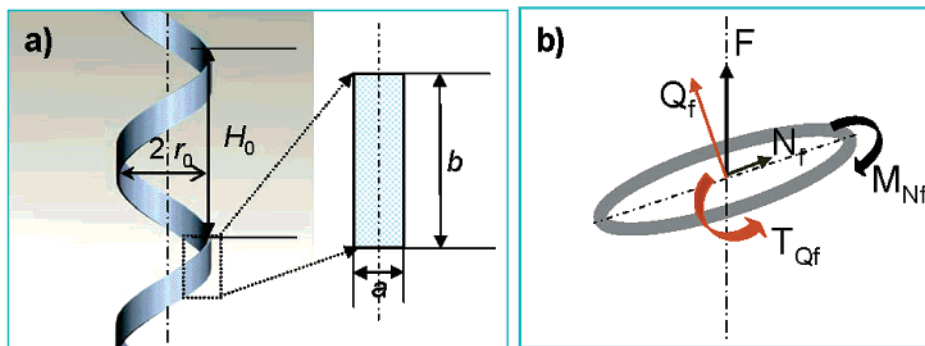
Figure 6. (a and b) Mechanical model of the nanohelix for calculating the spring constant as its radius changes during a uniaxial extension or compression. (c) A plot of the spring constant as a function of the dynamic radius, in which the length per turn of the coiled belt and shear modulus were assumed to be constant ($G = 70$ GPa) during extension or compression, the thickness of the coiled nanobelt $a = 20$ nm.

Table 1. Increase in Spring Constant for the Nanohelix at the Maximum Stretching: r_0, Original Radius without Deformation; r_f, Final Radius at Maximum Axial Stretching; K_0, Spring Constant at r_0; ϵ_{theory}, Relative Theoretical Maximum Elongation in Length; ϵ_{exper}, Relative Experimentally Observed Maximum Elongation; $\delta K/K_0$, Increase in Spring Constant.

N_1	$2r_0$ (nm)	$2r_f$ (nm)	H_0 (nm)	a (nm)	b (nm)	K_0 (N/m)	$\delta K/K_0$ (%)	ϵ_{theory} (%)	ϵ_{exper} (%)
2	980	190	2200	20	220	0.082	810	72.0	69.8
3	1100	500	3600	20	500	0.072	311	38.6	34.1
4	300	80	1000	20	380	2.71	651	37.4	35.1

Table 2. Characteristic Parameters of Nanohelix Used for Transverse Fracture Measurements by AFM.

N_2	F_1 (μN)	F_2 (μN)	$2r_0$ (nm)	H_0 (nm)	a (nm)	b (nm)
1	0.69	0.91	950	2200	20	380
2	1.34	–	960	1700	20	400
3	3.8	2.7	1200	3800	20	570
4	2.8	2.5	1000	3700	20	570
5	2.0	0.8	1100	2500	20	590
6	4.0	2.4	1100	2100	20	590
7	4.0	2.7	1100	2200	20	590

270 nm, then an eventual fracture occurred at 0.91 μN (IV stage of Figure 7d).

The origins that are responsible for the observed superelasticity can be suggested as two. One, the small thickness of the nanobelt making the nanohelix allows a large degree of deformation possible without introducing dislocation.[23] The small size leads to large degree of flexibility and elasticity. This is likely a common phenomenon at the
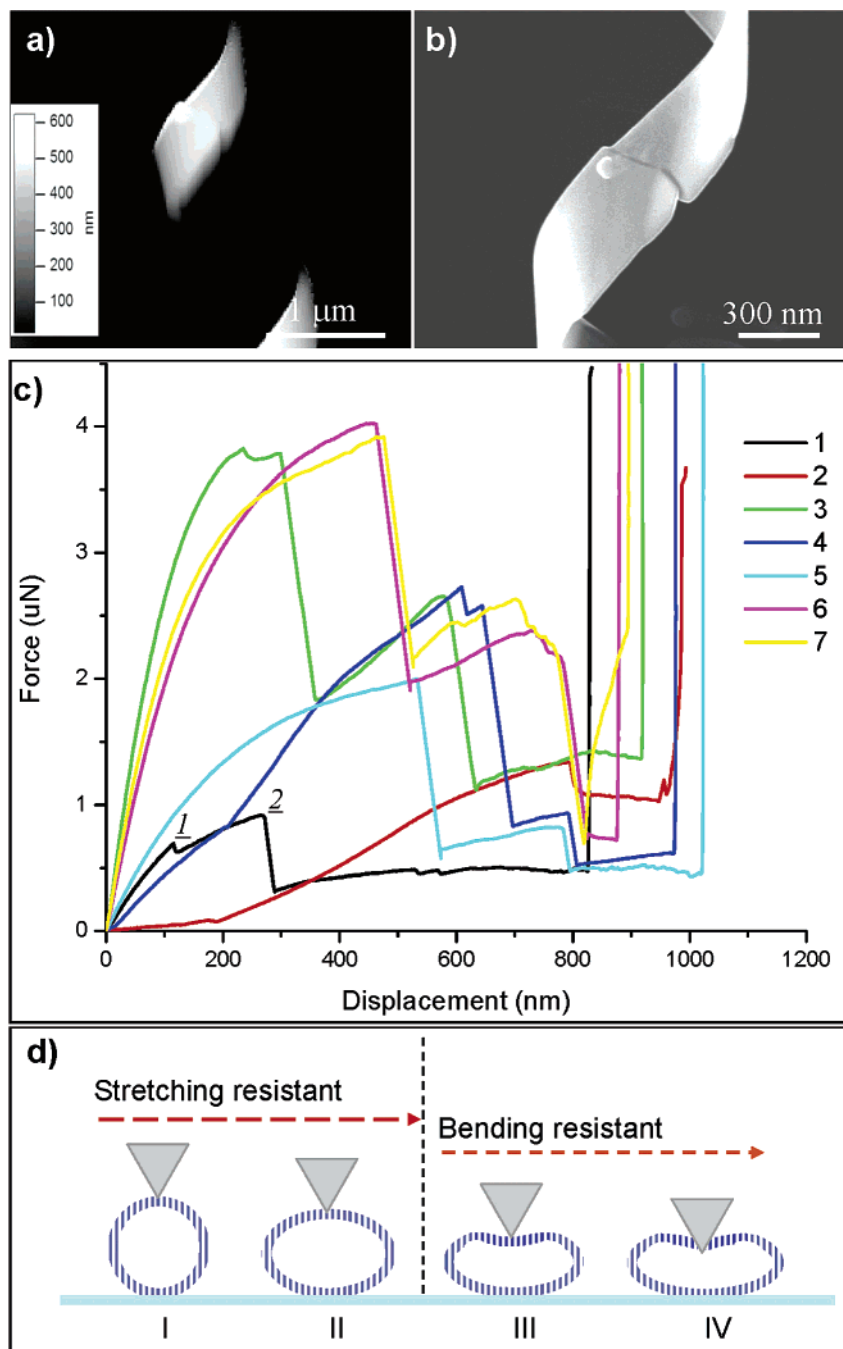
Figure 7. Two-step fracture process of nanohelices upon transversal compression by an AFM tip. Parts a and b are, respectively, an AFM topography image after the tip-induced fracture over a nanohelix and the corresponding SEM image of the fractured part. (c) Force-displacement curves for 7 nanohelices recorded during AFM tip compression and fracture process. (d) A schematic model of the two-step fracture process of the nanohelix upon transverse compression by an AFM tip.

nanoscale level. Last, the nanohelix is made of two types of parallel running stripes of ~3.5 nm in width,[16] which are ZnO but with different crystal orientations. The interface formed between the two types of stripes may absorb a large degree of deformation by atomic-scale twisting and bending. Such a process may not need to introduce dislocations. The curling of the nanobelt across the width is evidence of such bending.

Conclusions. In summary, a superelasticity (shape memory) effect has been discovered for the superlattice-structured ZnO nanohelices. By in situ manipulation using a nanoprobe, the

nanohelix could elastically recover its shape after an extremely large axial stretching, with an elastic elongation close to the theoretical limit, while suffering little residual plastic deformation. As a result of dynamic radius and pitch distance change in the course of mechanical stretching, the spring constant can be increased continuously up to 300−800% in reference to the value at low strain regime. It is suggested that the nanoscale thickness of the nanobelt and its superlattice structure might be the keys for the observed superelasticity. A shape memory/recovery of the nanohelix was observed after being subjected to a buckling deformation,

which provides direct experimental evidence of the buckling mechanism for explaining the force-displacement curve measured by the AFM tip.

The superelastic deformation and fracture process of a nanohelix have been studied by transversely compressing a nanohelix under the AFM tip. A two-step mechanism is suggested for explaining the measured force-displacement curve. When subjecting to a compression by the AFM tip, the nanohelix is suggested to be first undergoing a stretching process; then a bending deformation becomes dominant that introduces a buckling process, resulting in a sudden softening of the nanohelix. Continuous compressing results in a fracture at the contact point. But the shape of the nanohelix recovers after the fracture, suggesting that the nanohelix has a super large elasticity. The superelastic effect discovered in super-lattice-structured ZnO nanohelices may be a new category of shape-memory nanostructures made of ceramics, which could be of great interest for investigating the nanoscale fracture process and application in MEMS and NEMS. The elastic recovery of the nanohelix after extremely large deformation makes it a potential structure for nanoscale elastic energy storage. With an available high resonance frequency, the superelastic ZnO nanohelices can be made into smart microwave nanoantennas possibly with large bandwidths.[24]

References

(1) Davis, W. R.; Slawson, R. J.; Rigby, G. R. *Nature* **1953**, *171*, 756.
(2) Motojima, S.; Kawaguchi, M.; Nozaki, K.; Iwanaga, H. *Carbon* **1991**, *29*, 379.
(3) Zhang, L.; Deckardt, E.; Weber, A.; Schönenberger, C.; Grützmacher, D. *Nanotechnology* **2005**, *16*, 655.
(4) Zhang, L.; Ruh, E.; Grützmacher, D.; Dong, L.; Bell, D. J.; Nelson, B. J.; Schönenberger, C. *Nano Lett.* **2006**, *6*, 1311.
(5) Golod, S. V.; Prinz, V. Y.; Mashanov, V. I.; Gutakovsky, A. K. *Semicond. Sci. Technol.* **2001**, *16*, 181.
(6) Zhang, H. F.; Wang, C. M.; Buck, E. C.; Wang, L. S. *Nano Lett.* **2003**, *3*, 577.
(7) Qu, Y. Q.; Carter, J. D.; Guo, T. *J. Phys. Chem. B* **2006**, *110*, 8296.
(8) Zhang, H. F.; Wang, C. M.; Wang, L. S. *Nano Lett.* **2002**, *2*, 941.
(9) Wang, Z. L.; Kong, X. Y.; Ding, Y.; Gao, P. X.; Hughes, W. L.; Yang, R.; Zhang, Y. *Adv. Funct. Mater.* **2004**, *14*, 943.
(10) Kong, X. Y.; Ding, Y.; Yang, R.; Wang, Z. L. *Science* **2004**, *303*, 1348.
(11) Kong, X. Y.; Wang, Z. L. *Nano Lett.* **2003**, *3*, 1625.
(12) Gao, P. X.; Wang, Z. L. *Small* **2005**, *1*, 945.
(13) Shen, G. Z.; Bando, Y.; Zhi, C. Y.; Yuan, X. L.; Sekiguchi, T.; Golberg, D. *Appl. Phys. Lett.* **2006**, *88*, 243106.
(14) Prinz, V. Y.; Seleznev, V. A.; Gutakovsky, A. K.; Chehovskiy, A. V.; Preobrazhenskii, V. V.; Putyato, M. A.; Gavrilova, T. A. *Physica E* **2000**, *6*, 828.
(15) Bell, D. J.; Dong, L. X.; Nelson, B. J.; Golling, M.; Zhang, L.; Grutzmacher, D. *Nano Lett.* **2006**, *6*, 725.
(16) Gao, P. X.; Ding, Y.; Mai, W. J.; Hughes, W. L.; Lao, C. S.; Wang, Z. L. *Science* **2005**, *309*, 1700.
(17) Timoshenko, S.; Gere, J. *Mechanics of Materials*; Van Nostrand Reinhold Company: New York, 1972.
(18) Wahl, A. M. *Mechanical Springs*, 1st ed.; The Penton Publishing Company: Cleveland, OH, 1944.
(19) Chen, X.; Zhang, S.; Dikin, D. A.; Ding, W.; Ruoff, R. S.; Pan, L.; Nakayama, Y. *Nano Lett.* **2003**, *9*, 1299.
(20) Zaoui, A.; Sekkal, W. *Phys. Rev. B* **2002**, *66*, 174106.
(21) Lee, W.; Jeong, M.-C.; Myoung, J.-M. *Nanotechnology* **2004**, *15*, 254.
(22) Boudaoud, A.; Patricio, P.; Couder, Y.; Ben Amar, M. *Nature* **2002**, *407*, 718.
(23) Hughes, W. L.; Wang, Z. L. *J. Am. Chem. Soc.* **2004**, *126*, 6703.
(24) Wang, Z. L.; Gao, P. X.; Ding, Y. U.S. patent pending, 2005.

NL061943I